CHEMISTRY OF MATERIALS
Cite This: Chem. Mater. 2019, 31, 1628−1634
Article
pubs.acs.org/cm

# Highly Selective Radioactive $^{137}Cs^+$ Capture in an Open-Framework Oxysulfide Based on Supertetrahedral Cluster

Li Wang,*[,†,§] Huan Pei,[†] Debajit Sarma,[∥] Xian-Ming Zhang,*[,‡] Keith MacRenaris,[§] Christos D. Malliakas,[§] and Mercouri G. Kanatzidis*[,§]

[†]College of Chemistry & Chemical Engineering, Xinjiang Normal University, Urumqi 830054, P. R. China
[‡]School of Chemistry & Material Science, Shanxi Normal University, Linfen 041004, P. R. China
[§]Department of Chemistry, Northwestern University, Evanston, Illinois 60208, United States
[∥]Department of Chemistry, Indian Institute of Technology Patna, Bihta 801103, India

Supporting Information

**ABSTRACT:** Removal of $^{137}Cs^+$, one of the most hazardous radionuclides, from nuclear waste, is a challenging task because it requires simultaneously high capacity and high selectivity. Chalcogenides offer a great opportunity to design and create high-performance $^{137}Cs^+$ absorbents. We report a new material (InSnOS) with facile ion-exchange properties. The anionic framework is based on corner-shared pseudo-T4 supertetrahedral oxysulfide $[In_8Sn_{12}O_{10}S_{34}]^{16-}$ clusters, resulting in the formula $[In_8Sn_{12}O_{10}S_{32}]^{12-}$. The crystal structure features the interpenetration of two independent oxysulfide cluster frameworks which create pincer cavities based on sulfur atoms that prove highly effective for capturing $Cs^+$ ions. The binding mode of the $Cs^+$ ions by the material was determined by a single crystal structure refinement of a fully ion-exchanged single crystal. The structure determinations show that the small pores created by the two interpenetrating frameworks are the optimal size for capturing $Cs^+$. This advantage makes the material very effective for the removal and recovery of $^{137}Cs^+$ from aqueous solution. This framework shows not only extremely high exchange capacity ($q_m$), 537.7 mg per g of anionic $[In_8Sn_{12}O_{10}S_{32}]^{12-}$ framework, ranking it among the best reported $Cs^+$ sorbents, but also superior affinity and selectivity when using complex solutions simulating industrial and nuclear waste conditions.

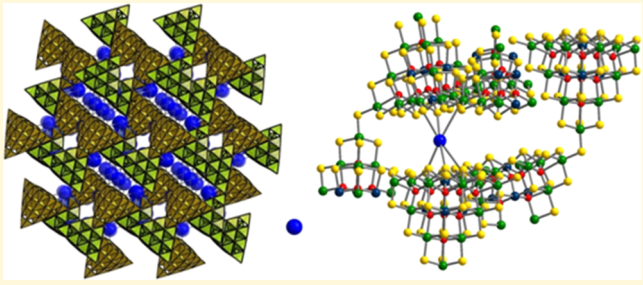

## INTRODUCTION

Nuclear power generation plays an indispensable role in meeting the world's increasing energy needs. The nuclear fuel cycle requires the removal and recovery of hazardous radionuclides from nuclear waste and the $^{137}Cs$ ion, the common fission product by the nuclear fission of uranium-235, is one of the most hazardous radionuclides because of its high fission yield (6.09%), long half-life (~30 years), and high solubility.[1−3] Thus, $^{137}Cs^+$ ions need to be removed effectively from nuclear waste solutions in the reprocessing plants using sorbents. The ideal $Cs^+$ sorbent must have (1) large exchange capacity, (2) high affinity and selectivity in solutions of extreme pH and very high salt concentrations, and (3) high structure stability.[4] A number of methods including ion exchange, precipitation, ultra-filtration, and solvent extraction have been developed for $^{137}Cs^+$ remediation.[5−11] Among these, ion capture or exchange are attractive because they promise low solidified waste volumes of radioactive discharge. Generally, ion capturers and exchangers can be divided into organic and inorganic materials.[12] The organic ion exchangers can potentially be destroyed in a highly radioactive solution by change and/or hydrolysis of functional groups, and thus inorganic ion exchangers are prominent for superior chemical, thermal, and radioactive stability as well as immobilization. Previously, inorganic oxides such as crystalline silicotitanate, zeolites, silicododecamolybdate, vanadosilicate (SGU-45), and clays were developed because of low cost.[2,5,13,14] However, they suffer from slow kinetics and low $Cs^+$ selectivity especially at high salt concentrations.

During the past several years, metal sulfide ion exchangers have emerged as a growing new class of materials that display exceptional selectivity and rapid sorption kinetics for soft or relatively soft metal ions. Recently, several metal sulfides with excellent $Cs^+$ adsorption properties have been reported, that is, KMS-1, KMS-2, KTS-1, KTS-3, FJSM-SnS etc.[15−21] Notably, most of these have layered anionic structures and labile interlayer cations. In addition, open-framework chalcogenides based on cluster building blocks with high negative charges, tunable pore size, high surface area, and high pore volume, can facilitate ion diffusion and ion-exchange kinetics throughout the pore systems of the crystals. These materials may be attractive for special applications in the separation of

Received: November 22, 2018
Revised: February 4, 2019
Published: February 5, 2019






DOI: 10.1021/acs.chemmater.8b04877
Chem. Mater. 2019, 31, 1628−1634

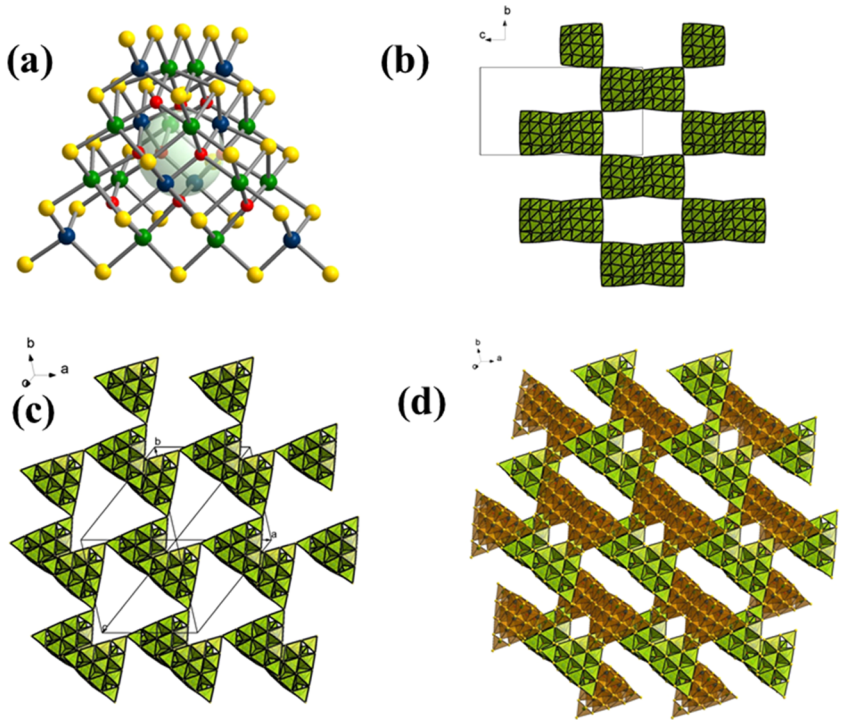


**Figure 1.** View of the pseudo-T4 supertetrahedral $[In_8Sn_{12}O_{10}S_{34}]^{16-}$ cluster with the missing $\mu_4$-S shown as a pale large dummy atom (a). Single set of cristobalite topological open-framework via corner sharing of clusters along the [100] (b) and [111] (c) directions, and interpenetration of two sets of frameworks (d) In, Sn, S, and O atoms are shown in deep blue, green, yellow, and red colors, respectively.

radionuclides and/or heavy metals from radioactive wastewater and other industrial wastewater.[21,22]

The chemical basis for the selectivity of sulfides is different from all materials developed previously and relies on the soft Lewis acid/base nature of the sorbent/$Cs^+$ interactions. In this work, we demonstrate a novel compound (InSnOS) with a pseudo-T4 supertetrahedral oxysulfide $[In_8Sn_{12}O_{10}S_{34}]^{16-}$ cluster framework with facile ion-exchange properties. The crystal structure features the interpenetration of two sets of independent oxysulfide cluster frameworks which create pincer cavities based on sulfur atoms that prove highly effective for capturing $Cs^+$ ions. The maximum $Cs^+$-exchange capacity ($q_m$) of InSnOS is 537.7(4.5) mg/g of the $[In_8Sn_{12}O_{10}S_{32}]^{12-}$ anionic framework, ranking it the highest among cesium sorbents. The material removes $Cs^+$ ions selectively in a simulated industrial and nuclear waste solution containing $Na^+$, $K^+$, $Mg^{2+}$, $Ca^{2+}$, and $NH_4^+$cations and $HCO_3^-$, $CO_3^{2-}$, $SO_4^{2-}$, $HPO_4^{2-}$, and $Cl^-$ anions in high as well as low concentrations.

## EXPERIMENTAL SECTION

**Synthesis.** A mixture of sulfur powder (0.0344 g, 1.07 mmol), $SnCl_2{\cdot}2H_2O$ (0.1523 g, 0.67 mmol), $In(NO_3)_3{\cdot}5H_2O$ (0.0982 g, 0.25 mmol), ethanolamine (eta) (4 mL), and water (2 mL) was placed into a 23 mL autoclave with a Teflon liner. The autoclave was heated at 160 °C for 4 days and then cooled to room temperature. A large number of colorless block-shaped crystals of InSnOS were obtained by filtration (Figure S1). The bulk phase purity was confirmed by the powder X-ray diffraction (PXRD) pattern (Figure S2). Elemental analyses for $(Heta)_{9.5}(H_3O)_{2.5}[In_8Sn_{12}O_{10}S_{32}]{\cdot}22H_2O$ (wt %): calcd C, 5.05; H, 2.68; N, 2.92; S, 22.48. Found: C, 5.07; H, 2.21; N, 2.78; S, 22.47.

**Ion-Exchange Experiments.** A typical ion-exchange experiment of dehydrated InSnOS with $Cs^+$ was carried out in a 20 mL vial, where the measured amount of CsCl was dissolved in deionized water (10 mL) and InSnOS (10 mg) was added. Then the mixture was kept under magnetic stirring from 30 min to 12 h at room temperature. InSnOS was centrifuged and isolated through filter paper (Whatman no. 1), washed several times with water and acetone, and dried in air. The concentrations of metal ions in the filtered solution were determined using inductively coupled plasma-atomic emission spectroscopy (ICP-OES) and, for extra low ion concentration (≤200 ppb), inductively coupled plasma-mass spectroscopy (ICP-MS).

The kinetic studies of $Cs^+$ ion exchange by InSnOS were carried out as follows. Ion-exchange experiments of various reaction times (5, 15, 30, 60, 120, 300 up to 1200 min) were performed. For each experiment, 10 mg of InSnOS was weighed and 10 mL sample of water solution containing 1 ppm of $Cs^+$ was added to each vial with $V/m$ = 1000 mL/g, and the mixtures were kept under magnetic stirring (pH = 7). The individual $Cs^+$ uptake from solutions of various concentrations was studied at room temperature. The data obtained were used for the determination of the sorption isotherms. All ion-exchange experiments here were performed by the batch method in 20 mL scintillation vials.

The individual ion-exchange experiments for $Cs^+$ ions at different pH values were also carried out. The required pH values (2, 4, 6, 8, 10, and 12) were achieved by diluting the commercial standards (1000 ppm) with HCl or NaOH solution to 5 ppm. The ion-exchange experiments at different salt concentrations were performed by dissolving the required amount of the corresponding salt in 10 mL solution of $Cs^+$ ion (about 5 ppm). The exchange experiments were performed with $V/m$ = 1000 mL/g at room temperature and 3−15 h contact.

**Characterization Techniques.** Single crystal X-ray diffraction data for the as-synthesized and various $Cs^+$-exchanged samples were collected at 100(2) K on an APEX II CCD diffractometer using monochromatic Mo K$\alpha$ radiation ($\lambda$ = 0.71073 Å) and integrated with the SAINT program. The structure was determined by direct methods and refined by full-matrix least-squares fitting on $F^2$. All calculations were performed with programs from the SHELXTL crystallographic software package.[23] All nonhydrogen atoms were refined with anisotropic thermal parameters. The solvent masking procedure as implemented in Olex2 was used to remove the electronic


DOI: 10.1021/acs.chemmater.8b04877
Chem. Mater. 2019, 31, 1628−1634

contribution of solvent molecules from the refinement. As the exact solvent content is not known, only the atoms used in the refinement model are reported in the formula here. The structure of the as-synthesized InSnOS was refined in the tetragonal space group $I4_1/acd$. Prior to solvent masking, the highest positive residual electron density due to solvent molecules was around 4 $e^-/Å^3$ for the pristine sample. Therefore, for the refinement of the Cs-exchanged crystals, electron densities located in the pores with values higher than 4 $e^-/Å^3$ were assigned as partially occupied Cs. The framework stoichiometry of samples soaked for 30 min to 2 weeks was found to vary in the range of $Cs_{9.4}In_8O_{10}S_{32}Sn_{12}$ to $Cs_{11.92}In_8O_{10}S_{32}Sn_{12}$. All Cs-exchanged structures were refined in the tetragonal space group $I4_1/acd$. Upon ion exchange, disorder was introduced in the crystal structure as suggested by the diffuse intensity present in the virtual precession images. Due to the disorder, agreement factors of a few sets of structures refined to larger values. Attempts to refine the structures to the lower symmetry orthorhombic space group *Ibca* did not yield significantly lower values, therefore all structures were refined in the tetragonal space group. Crystal data, details of data collection and structure refinement information are given in Table S1.

Powder X-ray diffraction (PXRD) patterns were collected on a CPS 120 INEL X-ray diffractometer using Cu K$\alpha$ radiation ($\lambda$ = 1.5418 Å) in the $2\theta$ angular range of 5−50°. Energy-dispersive spectroscopy (EDS) was performed with a Hitachi S-3400N-II scanning electron microscope equipped with an ESED II detector. An accelerating voltage of 20 kV and 60 s acquisition time were used for elemental analysis. The thermogravimetric (TG) analyses were carried out with a NETZSCH STA 449F3 simultaneous thermal analyzer instrument. The as-synthesized and $Cs^+$-exchanged samples and reference $Al_2O_3$ were enclosed in Pt crucibles, and heated from 25 to 800 °C at a heating rate of 10 °C/min under a nitrogen atmosphere. Infrared spectra were recorded on a Shimadzu IR Affinity-1 Fourier transform infrared spectrometer in the range from 400 to 4000 $cm^{-1}$ at room temperature. The samples were embedded in dried KBr matrixes, respectively. The concentrations of metal ions in the solution before and after $Cs^+$ ion-exchange were analyzed using ThermoFisher iCap7600 ICP-OES and ThermoFisher iCapQ ICP-MS instrumentation.

## RESULTS AND DISCUSSION

**Crystal Structure.** As-synthesized $(Heta)_{9.5}(H_3O)_{2.5}[In_8Sn_{12}O_{10}S_{32}]\cdot 22H_2O$ (InSnOS) crystallizes in the tetragonal space group $I4_1/acd$, with two In, three Sn, three O, and nine S crystallographically independent atoms in the asymmetric unit (Figure S3). This compound is isostructural to previous compound based on the $[In_4Sn_{16}O_{10}S_{34}]^{16-}$ cluster but has different In/Sn molar ratios and cationic templates.[24] The In(1) atom forms an $InS_4$ tetrahedron with In−S distances ranging from 2.372(4) to 2.441(3) Å. The In(2) atom is six coordinated by three S atoms and three O atoms, forming an $InS_3O_3$ octahedron with In−S distances ranging from 2.527(3) to 2.535(3) Å and In−O distances from 2.084(7) to 2.100(4) Å. The Sn(3), Sn(4), and Sn(5) sites show distorted octahedral geometries but are coordinated by four sulfur atoms and two oxygen atoms with Sn−S distances ranging from 2.429(3) to 2.577(3) Å and Sn−O distances from 2.101(1) to 2.429(8) Å. The In/Sn ratio of 2:3 was also determined using ICP-MS (Table S2).

The building block in InSnOS is the pseudo-T4 supertetrahedral $[In_8Sn_{12}O_{10}S_{34}]^{16-}$ cluster (Figure 1), which is composed of corner and edge-shared four $InS_4$, four $InS_3O_3$, and twelve $SnS_4O_2$ polyhedra. In the $[In_8Sn_{12}O_{10}S_{34}]^{16-}$ cluster, the 20 metal atoms can be represented as the cubic close-packed array (Figure S4). The 34 S atoms can be classified into three types, that is, 18 doubly bridging S atoms on the six edges, 12 triply bridging S atoms on 4 faces, and 4 terminal S atoms at the corners of the pseudo-T4 supertetrahedron. According to Pauling's electrostatic valence rule and Brown's equal valence rule, ideal T4 and even larger supertetrahedral clusters will be unstable for trivalent and tetravalent cations because of the presence of the divalent $\mu_4$-S atom bonded to four trivalent metal atoms. Nature herein selects the missing $\mu_4$-sulfur core and the presence of oxygen anions diverts excessive charge at the $\mu_3$-sulfur sites. In other words, the 34 sulfur atoms in the pseudo-T4 cluster are cubic close-packed but have a sulfide vacancy at the center to reduce the negative charge (Figure 1a).

The pseudo-T4 supertetrahedral clusters are corner-shared into a three-dimensional (3D) cristobalite-type topological motif (Figure 1b,c). Within the $SiO_2$ cristobalite architecture, the pseudo-T4 clusters occupy the Si sites and the corner-sharing sulfides occupy the −O− sites. As can be seen, a single framework gives rectangular channels sized ca. 20.9 Å × 11.2 Å along the *a*- and *b*-axis directions. Notably, there are larger equilateral triangular channels along the [111] direction and the side length of equilateral triangle is about 26.3 Å (without considering atomic van der Waals radii). The overall structure is 2-fold interpenetrated but still has 53% of void space filled by organic templates and solvents. IR (Figure S5), TG (Figure S6), and elemental analysis combined single crystal diffraction to establish the formula of $(Heta)_{9.5}(H_3O)_{2.5}[In_8Sn_{12}O_{10}S_{32}]\cdot 22H_2O$. The solvent water molecules can be removed under vacuum over 2 days to generate dehydrated $(Heta)_{9.5}(H_3O)_{2.5}[In_8Sn_{12}O_{10}S_{32}]$ which were confirmed by the powder XRD and elemental analyses (Figure S2 and Table S4). There are approximately 20 Å × 6 Å rectangular channels along the [111] direction after 2-fold interpenetration (Figure 1d). The guest molecules filling the pores were not located due to the statistical disorder usually encountered in this kind of structure. As shown in Figure S2, the observed XRD patterns are in good agreement with the corresponding theoretical ones. Thermal gravimetric measurements on InSnOS showed two weight loss steps associated with the removal of guests, that is, (a) 7.5% below 120 °C because of the removal of water molecules and (b) 12.5% between 200 and 400 °C attributed to the decomposition of ethanolaminium. Compared with the as-synthesized sample, $Cs^+$-exchanged InSnOS shows one stepped weight loss of 12.6% below 130 °C associated with the removal of water molecules (Figure S6).

**Single Crystal to Single Crystal $Cs^+$ Exchange.** The crystal structures of $Cs^+$-exchanged InSnOS could be determined by X-ray single crystal diffraction analyses since a complete single crystal to single crystal ion exchange is rapid and does not destroy the crystals (Figure S1). The X-ray crystallographic refinements reveal how the 2-fold interpenetrated open oxysulfide framework of InSnOS captures the $Cs^+$ ions. The $Cs^+$-exchanged crystals obtained from ion-exchange reactions with aqueous CsCl solution at room temperature for 0.5 h, 1 h, 3 h, and 2 weeks are referred to as InSnOS-0.5h, InSnOS-1h, InSnOS-3h, and InSnOS-2w, respectively. Table S1 gives the crystal data and structure refinement for InSnOS and $Cs^+$-exchanged crystals. As can be seen from simulated precession photographs of the reciprocal space for an InSnOS crystal before and after soaking in CsCl, the long-range crystallinity is retained after the ion-exchange process (Figure S7). Herein, we take InSnOS-0.5h as an example to describe the pincer action resulting from the interactions between sulfur atoms in the framework and the captured $Cs^+$.


DOI: 10.1021/acs.chemmater.8b04877
*Chem. Mater.* 2019, 31, 1628−1634

There are 14 crystallographically independent Cs sites in the asymmetric unit as shown in Figure S8. All 14 Cs sites show binding interactions with sulfur atoms from the oxysulfide framework with Cs···S distances in the range of 3.5−4.0 Å (Figure 2). There is much more room available than required

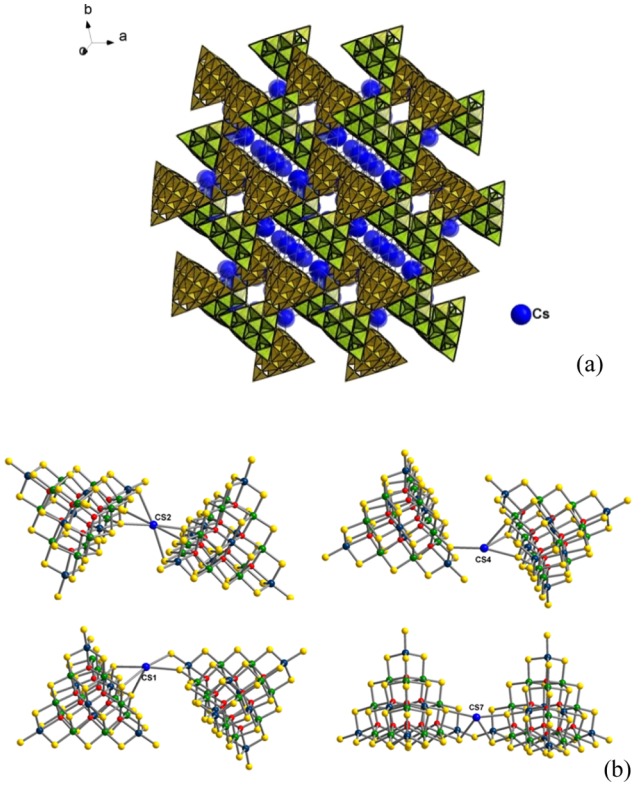


**Figure 2.** (a) Three-dimensional (3D) structure of InSnOS-0.5h showing $Cs^+$ (blue atoms) captured by two sets of metal oxysulfide open frameworks along the [111] direction. (b) View of representative local sulfur based environment sites for binding $Cs^+$ in the $Cs^+$-exchanged InSnOS-0.5h crystal.

by the incoming $Cs^+$ cations, and they become positionally disordered and mobile. Because of its large ionic radius, the $Cs^+$ show variable coordination numbers. The few disordered water molecules which may supplement the coordination sphere of some of the $Cs^+$ could not be located in the Fourier map due to very low electronic density. The $Cs^+$ show the following Cs···S interacting features. (i) Each Cs is bonded to at least two sulfur atoms from at least two pseudo-T4 clusters; (ii) all Cs ions tend to be chelated by two or three sulfur atoms from a pseudo-T4 cluster; (iii) the *n*S ($n$ = 2−6)-based coordination polyhedra around Cs ions are diverse, i.e., linear 2S, trigonal 3S, tetrahedral 4S, butterfly 4S, irregular 5S, and octahedral 6S; (iv) two pseudo-T4 clusters bond to one Cs ion one from each of the two independent cristobalite-like open frameworks. It should be particularly pointed out that Cs(2) has an octahedral coordination geometry, being chelated by two $\eta^3$-pseudo-T4 supertetrahedral clusters. From the above description, we clearly see that it is the inherent interpenetration of two independent frameworks in InSnOS that creates multiple types of sulfide-based binding pockets acting as pincers for the capture of $Cs^+$. The refinement of structures for $Cs^+$-exchanged crystals performed at different soaking times indicated a dynamic nature of the lattice with slight differences in captured $Cs^+$, although all structures showed similar $Cs^+$ coordination environments (Figures S9−S12).

Layered metal sulfides, such as KMS-1, KMS-2, KTS-3, and FJSM-SnS, have also been studied for radionuclide capture.[22] In particular, Kanatzidis et al reported KTS-3 as a material with excellent $Cs^+$ ion-exchange properties in varying conditions, which has a unique anionic layer structure consisting of $[SnS_6]$ octahedra, $[SnS_4]$ tetrahedra, and long range ordered vacancies in the $[SnS_4]$.[18,23] The properties of InSnOS are reminiscent of those of the layered ion-exchange compound $[(CH_3)_2NH_2]_2[Ga_2Sb_2S_7]_2$ layers which via its framework flexibility selectively captures Cs ions in a manner similar to a Venus flytrap.[24]

**Batch $Cs^+$-Exchange Properties.** *Kinetics and Isotherm.* The kinetic studies of the $Cs^+$ exchange indicate that the concentrations of $Cs^+$ (1000 ppb) ions decreased sharply and reached equilibrium within 5 min at room temperature, Figure 3a. This should be attributed to the large channel window of

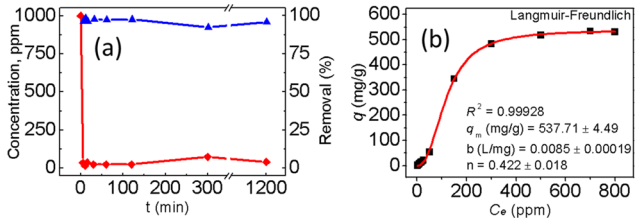


**Figure 3.** (a) Kinetics of the $Cs^+$ ion-exchange process plotted as the $Cs^+$ concentration (ppb) and the relative amount of Cs removed (%) vs the time $t$ (min), respectively. (b) The $Cs^+$ equilibrium curve for InSnOS (pH = 7, $V/m$ = 1000 mL/g, contact time 20 min, at room temperature, initial $Cs^+$ concentration in the range of 1−1000 ppm). The Langmuir equilibrium isotherm derived from the $Cs^+$ concentration at equilibrium plotted against the capacity.

InSnOS and unique sulfide-based pockets acting as pincers for soft $Cs^+$ ions. To evaluate the absorption capacity of InSnOS for $Cs^+$, we carried out absorption isotherm experiments with various concentrations of cesium (1−1000 ppm) in pH ∼7 at room temperature. The $Cs^+$ equilibrium curve shown in Figure 3b derives from the concentration at equilibrium plotted against the capacity of $Cs^+$ exchange. The Langmuir−Freundlich equilibrium isotherm model fits very well with a good correlation coefficient. The maximum $Cs^+$-exchange capacity ($q_m$) of InSnOS was found to be 537.7(4.5) mg/g, ranking it among the best reported $Cs^+$ adsorbents and much higher than those of commercial $Cs^+$ sorbents[8−11,14−16,25] (Table S3). The ion-exchange processes can be described by the following equation

$$(\text{Heta})_{9.5}(H_3O)_{2.5}[In_8Sn_{12}O_{10}S_{32}] + 12\ Cs^+ + xH_2O \rightarrow Cs_{12}[In_8Sn_{12}O_{10}S_{32}]\cdot xH_2O + 9.5(\text{Heta})^+ + 2.5H_3O^+$$

The measured $q_m$ of 537.7 mg/g of $[In_8Sn_{12}O_{10}S_{32}]^{12-}$ open anionic framework is larger than that of the theoretical capacity for $Cs^+$ (452 mg/g calculated from per gram of anhydrous open oxysulfide anionic framework). The latter is calculated under the assumption that only organic cations and protonated water in pores are exchangeable. The theoretical capacity is related to the pore adsorption (i.e., exchange of guest cations by $Cs^+$ which occurs inside the pores of InSnOS). Here, the higher $Cs^+$-exchange capacity than theoretical in InSnOS may result from surface adsorption. Furthermore, compared with


DOI: 10.1021/acs.chemmater.8b04877
Chem. Mater. 2019, 31, 1628−1634

pristine InSnOS, the C and N fraction in elemental analyses of the $Cs^+$-exchanged product is strongly decreased, consistent with full $Cs^+$ exchange (Table S4). IR spectroscopy of the $Cs^+$-exchanged product indicates the near absence of N−H bending vibration at 1570 $cm^{-1}$ and the C−N stretching vibration at 1150 $cm^{-1}$ (Figure S5). The $Cs^+$ ion-exchanged material was also characterized by EDS (Figure S13), which clearly showed homogeneous distribution of Cs, In, and Sn, throughout the crystals, and no N fraction in the $Cs^+$-exchanged product could be detected which confirms that guest cations in the pores are fully exchanged by $Cs^+$. In addition, the PXRD patterns of the ion-exchanged products were similar to those of the pristine InSnOS sample (Figure S2). Figure S1 shows the single crystal images of pristine InSnOS and $Cs^+$-exchanged products.

*pH-Dependent Studies.* The distribution coefficient $K_d$ was measured over a broad pH range (2−12). $K_d$ is a measurement of affinity and selectivity, described by eq 1. The ion-exchange efficiency, i.e., the relative amount of removed ($R$), was calculated with eq 2. In eqs 1 and 2, $C_0$ and $C_f$ represent the initial and equilibrium concentrations of the ions as measured by ICP.

$$K_d = \frac{V}{m}\frac{(C_0 - C_f)}{C_f} \quad (1)$$

$$R = \frac{(C_0 - C_f)}{C_0} \times 100\% \quad (2)$$

pH-dependent ion-exchange feature is performed with $Cs^+$ solutions ($Cs^+$ concentration is 5 ppm, $V/m$ = 1000 mL/g) of various pH values with a very high percentage of Cs removal (>93.2%) and the high $K_d$ values ranging from $1.37 \times 10^4$ to $1.98 \times 10^4$ mL/g in the pH range of 4−10 (Figure 4). Even in

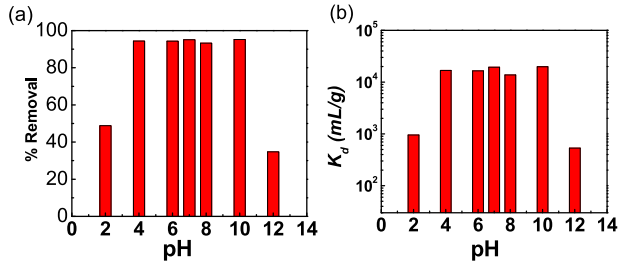


**Figure 4.** Variation of removal efficiency (a) and distribution coefficient $K_d$ (b) with pH.

relatively strong acid and strong alkali solution (pH = 4 or pH = 10), the relative amounts of $Cs^+$ removed can reach 94.4 and 95.1%, and $K_d$ values can reach $1.69 \times 10^4$ and $1.98 \times 10^4$ mL/g, respectively. In general, a material with a $K_d$ value >$10^4$ mL/g is considered to be an excellent adsorbent.[7] Clearly, InSnOS is effective in removing $Cs^+$ in acidic, neutral, and alkali conditions. Powder XRD patterns of $Cs^+$-exchanged products in the pH range of 2−12 confirm the stability of compound (Figure S2). This performance is superior to many oxide ion exchangers such as manganese oxides and titanate.[18]

*Selectivity Studies.* Since in industrial and nuclear waste a broad concentration range of other non-radioactive cations such as $Na^+$, $K^+$, $Mg^{2+}$, $Ca^{2+}$, and $NH_4^+$ and anions $HCO_3^-$, $CO_3^{2-}$, $SO_4^{2-}$, $HPO_4^{2-}$, and $Cl^-$ are present,[25,26] the performance of InSnOS for $Cs^+$ ion exchange in the presence of a variety of concentrations of all these ions were tested (Figures 5 and S15). The capture performance of InSnOS for $Cs^+$ (5 ppm) is impressive in the presence of $Na^+$, $K^+$, $Mg^{2+}$,

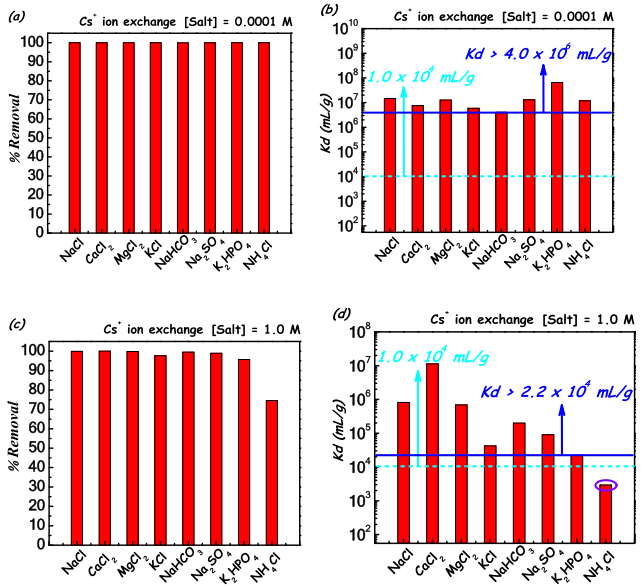


**Figure 5.** Variation of removal efficiency and distribution coefficient $K_d$ with different molar concentrations of NaCl, $CaCl_2$, $MgCl_2$, KCl, $NaHCO_3$, $Na_2SO_4$, $K_2HPO_4$, and $NH_4Cl$.

$Ca^{2+}$, and $NH_4^+$cations and $HCO_3^-$, $CO_3^{2-}$, $SO_4^{2-}$, $HPO_4^{2-}$, and $Cl^-$ anions from low to high concentration (0.0001, 0.001, 0.01, 0.1, and 1 M, respectively). In the presence of 0.0001, 0.001, and 0.01 M concentrations of $Na^+$, $K^+$, $Mg^{2+}$, $Ca^{2+}$, and $NH_4^+$cations and $HCO_3^-$, $CO_3^{2-}$, $SO_4^{2-}$, $HPO_4^{2-}$, and $Cl^-$ anions, InSnOS maintains an exceptional ability to selectively absorb $Cs^+$ (≥99.9% $Cs^+$ removal capacity, $K_d$ values higher than $9.7 \times 10^5$ mL/g). At a higher concentration of 0.1 M ions, the $Cs^+$ removal capacity is >99.4%, and the corresponding $K_d$ values were >$1.7 \times 10^5$ mL/g. Even at a very high concentration of 1 M of $Na^+$, $K^+$, $Mg^{2+}$, and $Ca^{2+}$cations and $HCO_3^-$, $CO_3^{2-}$, $SO_4^{2-}$, $HPO_4^{2-}$, and $Cl^-$ anions ($2.7 \times 10^4$-fold-to $Cs^+$), InSnOS could still exhibit ≥95.7% $Cs^+$ removal capacity with large $K_d$ values ≥$2.2 \times 10^4$ mL/g. It should be pointed out that we observed an abnormal and relatively low removal efficiency of $Cs^+$ in 1 M $NH_4^+$, which may be due to the high concentration of $NH_4^+$ pushing some $Cs^+$ out in a back ion-exchange process. Interestingly, the ion exchange ability of InSnOS in the presence of high salt concentration is higher than in pure water.

This increased ion exchange in the presence of various cations and anions may be promoted by the very high salt concentration of the other cations which may enter the pores of InSnOS first to exchange with the organic cations (kinetic control). Subsequently, these kinetically labile and fast entering $Na^+$ and $Ca^{2+}$ ions are exchanged out by the softer Lewis acid $Cs^+$ ions due to stronger bonding interaction with the soft basic ($S^{2-}$) sites (thermodynamic control). That is, this could be a combined kinetic and thermodynamic effect, in which first the highly labile $Na^+$ and $Ca^{2+}$ exchange the organic counterions and in a second step these are exchanged by the more chalcophilic (softer) $Cs^+$ cations. There are rectangular channels along the [111] direction after 2-fold interpenetration in this framework (approximate 20 Å × 6 Å), which provide plenty of binding sites to capture $Cs^+$. Taking into account the


DOI: 10.1021/acs.chemmater.8b04877
Chem. Mater. 2019, 31, 1628−1634

distances of Cs···S in the range of 3.5−4.0 Å and the fact that $Cs^+$ are chelated by two or more sulfur atoms ($n$ = 2−6), the channels have the proper size to act as pincers for selective capture of the size matched $Cs^+$ ions (Figures 2 and 6).

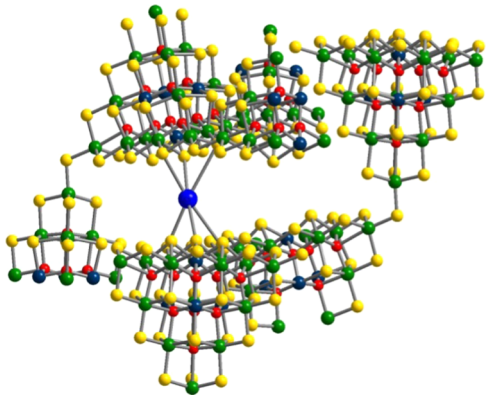

**Figure 6.** View of the local binding environment of the Cs ion in the pore of the Cs-exchanged InSnOS-0.5h crystal.

There are similar instances in the literature where the sorbent material is reported to exhibit higher ion exchange ability in the presence of high salt concentrations than in pure water. For example, Ma et al. demonstrated fast, highly efficient concurrent removal of toxic oxoanions of Se(VI) ($SeO_4^{2-}$) and Se(IV) ($SeO_3^{2-}$/$HSeO_3^-$) and heavy metal ions of $Hg^{2+}$, $Cu^{2+}$, and $Cd^{2+}$ by the $MoS_4^{2-}$-intercalated Mg/Al-layered double hydroxide (MgAl-$MoS_4$-LDH, abbr. $MoS_4$-LDH). When $Hg^{2+}$ (20 ppm) coexisted with $SeO_4^{2-}$, an increased maximum capacity of ∼102 mg/g for Se(VI) was obtained, suggesting the binding metal ions to be $MoS_4^{2-}$, preventing its release.[27]

## CONCLUSIONS

To conclude, we described a unique material featuring two-fold interpenetrated supertetrahedral oxysulfide $[In_8Sn_{12}O_{10}S_{34}]^{16-}$ cluster-based frameworks having small pore pockets created by the two frameworks. These pockets act as pincers for selectively capturing $Cs^+$ ions even in the presence of very high concentrations of other ions and over a wide pH range. This new compound exhibits an exchange capacity ($q_m$), of 537.7 mg/g of anionic framework, ranking it among the best reported $Cs^+$ adsorbents.

## ASSOCIATED CONTENT

### Supporting Information

The Supporting Information is available free of charge on the ACS Publications website at DOI: 10.1021/acs.chemmater.8b04877.

Final coordinates, selected bond distances, bond angles, XRD, IR, TG, elemental analysis, EDS, electron localization function map; CCDC deposition number of InSnSO-Cs-0.5h, InSnSO, InSnSO-Cs-3h, InSnSO-Cs-2w, and InSnSO-Cs-1h are 1825665-1825669 (PDF) Crystallographic data (CIF) (CIF) (CIF) (CIF) (CIF)

## AUTHOR INFORMATION


### Corresponding Authors

*E-mail: wangliresearch@163.com (L.W.).
*E-mail: zhangxm@dns.sxnu.edu.cn (X.-M.Z.).
*E-mail: m-kanatzidis@northwestern.edu (M.G.K.)

### ORCID

Li Wang: 0000-0002-7425-6872
Xian-Ming Zhang: 0000-0002-8809-3402
Christos D. Malliakas: 0000-0003-4416-638X
Mercouri G. Kanatzidis: 0000-0003-2037-4168


### Author Contributions

L.W., X.-M.Z., and M.G.K. planned the research and L.W. prepared the manuscript. L.W. performed the single crystal and powder InSnOS $Cs^+$-exchanged ion exchange experiments, including kinetic studies, isotherm experiments, effects of cations, anions, pH, XRD, TG, and IR characterization. H.P. synthesized InSnOS. S.D. gave the suggestion during experiments and did the EDS characterization. L.W., X.-M.Z., and C.D.M. performed X-ray single structural analyses. M.K. helped the ICP measurements. All authors discussed the results and commented on the manuscript.

### Notes

The authors declare no competing financial interest.

## ACKNOWLEDGMENTS

This work is supported by the National Science Foundation (Grant DMR-1708254), the NSFC (51762039 and 21871167), 1331 project, National Plan for 10 000 Talents in China, and 2017XS03.

## REFERENCES


(1) Awual, M. R.; Suzuki, S.; Taguchi, T.; Shiwaku, H.; Okamoto, Y.; Yaita, T. Radioactive cesium removal from nuclear wastewater by novel inorganic and conjugate adsorbents. *Chem. Eng. J.* **2014**, *242*, 127−135.

(2) El-Kamash, A. M. Evaluation of zeolite A for the sorptive removal of $Cs^+$ and $Sr^{2+}$ ions from aqueous solutions using batch and fixed bed column operations. *J. Hazard. Mater.* **2008**, *151*, 432−445.

(3) Yasunari, T. J.; Stohl, A.; Hayano, R. S.; Burkhart, J. F.; Eckhardt, S.; Yasunari, T. Cesium-137 deposition and contamination of Japanese soils due to the Fukushima nuclear accident. *Proc. Natl. Acad. Sci. U.S.A.* **2011**, *108*, 19530−19534.

(4) Wang, Y. L.; Liu, Z. Y.; Li, Y. X.; Bai, Z. L.; Liu, W.; Wang, Y. X.; Xu, X. M.; Xiao, C. L.; Sheng, D. P.; Juan, D. W.; Su, J.; Chai, Z. F.; Albrecht-Schmitt, T. E.; Wang, S. Umbellate Distortions of the Uranyl Coordination Environment Result in a Stable and Porous Polycatenated Framework That Can Effectively Remove Cesium from Aqueous Solutions. *J. Am. Chem. Soc.* **2015**, *137*, 6144−6147.

(5) Behrens, E. A.; Clearfield, A. Titanium silicates, $M_3HTi_4O_4(SiO_4)_3$ $4H_2O$ (M = Na+, K+), with three-dimensional tunnel structures for the selective removal of strontium and cesium from wastewater solutions. *Microporous Mater.* **1997**, *11*, 65−75.

(6) Behrens, E. A.; Sylvester, P.; Clearfield, A. Assessment of a sodium nonatitanate and pharmacosiderite-type ion exchangers for strontium and cesium removal from DOE waste simulants. *Environ. Sci. Technol.* **1998**, *32*, 101−107.

(7) Sharma, S.; Singh, B.; Manchanda, V. K. Phytoremediation: role of terrestrial plants and aquatic macrophytes in the remediation of radionuclides and heavy metal contaminated soil and water. *Environ. Sci. Pollut. Res.* **2015**, *22*, 946−962.

(8) Thiessen, K. M.; Thorne, M. C.; Maul, P. R.; Prohl, G.; Wheater, H. S. Modelling radionuclide distribution and transport in the environment. *Environ. Pollut.* **1999**, *100*, 151−177.

(9) Wilmarth, W. R.; Lumetta, G. J.; Johnson, M. E.; Poirier, M. R.; Thompson, M. C.; Suggs, P. C.; Machara, N. P. Review: Waste-Pretreatment Technologies for Remediation of Legacy Defense Nuclear Wastes. *Solvent Extr. Ion Exch.* **2011**, *29*, 1−48.

(10) Romanovskiy, V. N.; Smirnov, I. V.; Babain, V. A.; Todd, T. A.; Herbst, R. S.; Law, J. D.; Brewer, K. N. The universal solvent extraction (UNEX) process. I. Development of the UNEX process




DOI: 10.1021/acs.chemmater.8b04877
*Chem. Mater.* 2019, 31, 1628−1634

solvent for the separation of cesium, strontium, and the actinides from acidic radioactive waste. *Solvent Extr. Ion Exch.* **2001**, *19*, 1−21.
(11) Haas, P. A. A Review Of Information On Ferrocyanide Solids For Removal Of Cesium From Solutions. *Sep. Sci. Technol.* **1993**, *28*, 2479−2506.
(12) Awual, M. R.; Miyazaki, Y.; Taguchi, T.; Shiwaku, H.; Yaita, T. Encapsulation of cesium from contaminated water with highly selective facial organic-inorganic mesoporous hybrid adsorbent. *Chem. Eng. J.* **2016**, *291*, 128−137.
(13) Datta, S. J.; Moon, W. K.; Choi, D. Y.; Hwang, I. C.; Yoon, K. B. A Novel Vanadosilicate with Hexadeca-Coordinated Cs+ Ions as a Highly Effective Cs+ Remover. *Angew. Chem., Int. Ed.* **2014**, *53*, 7203−7208.
(14) He, Q.; Walling, D. E. Interpreting particle size effects in the adsorption of Cs-137 and unsupported Pb-210 by mineral soils and sediments. *J. Environ. Radioact.* **1996**, *30*, 117−137.
(15) Manos, M. J.; Kanatzidis, M. G. Highly Efficient and Rapid $Cs^+$ Uptake by the Layered Metal Sulfide $K_{2x}Mn_xSn_{3-x}S_6$ (KMS-1). *J. Am. Chem. Soc.* **2009**, *131*, 6599−6607.
(16) Manos, M. J.; Kanatzidis, M. G. Sequestration of Heavy Metals from Water with Layered Metal Sulfides. *Chem. - Eur. J.* **2009**, *15*, 4779−4784.
(17) Mertz, J. L.; Fard, Z. H.; Malliakas, C. D.; Manos, M. J.; Kanatzidis, M. G. Selective Removal of Cs+, Sr2+, and Ni2+ by $K_{2x}Mg_xSn_{3-x}S_6$ (x = 0.5−1) (KMS-2) Relevant to Nuclear Waste Remediation. *Chem. Mater.* **2013**, *25*, 2116−2127.
(18) Sarma, D.; Malliakas, C. D.; Subrahmanyam, K. S.; Islama, S. M.; Kanatzidis, M. G. $K_{2x}Sn_{4-x}S_{8-x}$ (x = 0.65−1): a new metal sulfide for rapid and selective removal of $Cs^+$, $Sr^{2+}$ and $UO_2^{2+}$ ions. *Chem. Sci.* **2016**, *7*, 1121−1132.
(19) Feng, M. L.; Sarma, D.; Qi, X. H.; Du, K. Z.; Huang, X. Y.; Kanatzidis, M. G. Efficient Removal and Recovery of Uranium by a Layered Organic-Inorganic Hybrid Thiostannate. *J. Am. Chem. Soc.* **2016**, *138*, 12578−12585.
(20) Qi, X. H.; Du, K. Z.; Feng, M. L.; Gao, Y. J.; Huang, X. Y.; Kanatzidis, M. G. Layered $A_2Sn_3S_7$ -1.25$H_2O$ (A = Organic Cation) as Efficient Ion Exchanger for Rare Earth Element Recovery. *J. Am. Chem. Soc.* **2017**, *139*, 4314−4317.
(21) Feng, M. L.; Sarma, D.; Gao, Y. J.; Qi, X. H.; Li, W. A.; Huang, X. Y.; Kanatzidis, M. G. Efficient Removal of UO2 (2+), Cs+, and Sr2+ Ions by Radiation-Resistant Gallium Thioantimonates. *J. Am. Chem. Soc.* **2018**, *140*, 11133−11140.
(22) Manos, M. J.; Ding, N.; Kanatzidis, M. G. Layered metal sulfides: Exceptionally selective agents for radioactive strontium removal. *Proc. Natl. Acad. Sci. U.S.A.* **2008**, *105*, 3696−3699.
(23) Sarma, D.; Islam, S. M.; Subrahmanyam, K. S.; Kanatzidis, M. G. Efficient and selective heavy metal sequestration from water by using layered sulfide K2xSn4-xS8-x (x = 0.65−1; KTS-3). *J. Mater. Chem. A* **2016**, *4*, 16597−16605.
(24) Ding, N.; Kanatzidis, M. G. Selective incarceration of caesium ions by Venus flytrap action of a flexible framework sulfide. *Nat. Chem.* **2010**, *2*, 187−191.
(25) Carey, T.; Williams, C. D.; McArthur, D. J.; Malkinson, T.; Thompson, O. R.; Baidak, A.; Murtagh, L.; Glodan, G.; Morgan, S. P.; Banford, A. W. Removal of Cs, Sr, U and Pu species from simulated nuclear waste effluent using graphene oxide. *J. Radioanal. Nucl. Chem.* **2018**, *317*, 93−102.
(26) Jena, H.; Raghavan, S.; Pogaku, V.; Bandi, P. R.; Vadakkapet, G. K. K. Removal of Ru from Simulated High-Level Waste Prior to the Final Vitrification into Borosilicate Glass Using Tin as the Alloying Element: Feasibility Study. *J. Hazard., Toxic Radioact. Waste* **2018**, *22*, No. 04018018.


DOI: 10.1021/acs.chemmater.8b04877
*Chem. Mater.* 2019, 31, 1628−1634